A mesoscale compliant expansion chamber for a catalytic micro-engine

Basile, Serena; Goosen, Johannes F.L.

DOI
10.1016/j.mne.2025.100339

Publication date
2025

Document Version
Final published version

Published in
Micro and Nano Engineering

MNE 29 (2025) 100339

Contents lists available at ScienceDirect

Micro and Nano Engineering

journal homepage: www.sciencedirect.com/journal/micro-and-nano-engineering

A mesoscale compliant expansion chamber for a catalytic micro-engine☆

Serena Basile[a,b,*], Johannes F.L. Goosen[a]

[a] Department of Precision and Microsystem Engineering, Delft University of Technology, Delft 2628 CD, the Netherlands
[b] Research and Innovation Centre Techniek, Ontwerpen en Informatica, Inholland University of Applied Sciences, 1817MN Alkmaar, the Netherlands

A B S T R A C T

As engineering applications become increasingly complex, the need for miniaturization is present in several technological fields. Places hardly reachable by traditional tools and machines, can be accessed thanks to miniaturized devices and, especially when such devices are remotely controlled or autonomous, it implies the need for miniaturized, standalone actuators. Most high-energy density actuators for these applications can not be operated if untethered from an external power-supply.

In this study, we investigate the manufacturing of a mesoscale compliant expansion chamber for a miniaturized chemical-based actuator. Photopolymerization and material jetting are used for manufacturing the prototypes, exhibiting dimensions of 9.8 mm diameter, 7.5 mm height and 140 μm thickness. These dimensions are such as to allow the device to fit inside of the flapping wings micro aerial vehicle (FWMAV) that it has to power. Fabrication of such dimensions, along with the peculiar geometry of the chamber, taps into the limitations of the photopolymerization process and highlights areas of improvement for this rapidly-developing technology. The devices are successfully tested for a linear motion, mimicking that of a cylinder-piston combination, as in a conventional expansion chamber, and are actuated by a pressure pulse.

Introduction

With the continuous development of microelectronics, micro-systems, microsensors and micro-robots, increasingly complex tasks including mechanical actuation, signal detection, medical procedures and information processing can be accomplished [1]. Miniaturized devices can conveniently monitor the environment, agriculture and urban areas, and in some instances, automation and autonomy are included to facilitate the process and increase adaptability. Significantly, the power supply is key to the autonomy and functionality of miniature systems. Although various forms of energy can be used, ensuring a lightweight and portable power unit with high capability in terms of energy and power density, is a necessary step for the usability of such technologies. This holds in particular when considering technologies whose operation modes and conditions are exceptionally power-hungry. For example, in the last years drones are used in an increasing number of roles, ranging from security to leisure. This has brought also the need of developing a variety of sizes and technologies. While rotary-wing drones still cover the majority of the aerial vehicles on the market, different and more bio-inspired alternatives are being studied, developed and commercialised. These are commonly named flapping-wings aerial vehicles (FWAV) where, as the name suggests, the generation of the lift happens through flapping wings rather than in the more conventional rotary-wing drones. FWAV advantages include higher robustness, manoeuvrability and efficient forward flight, while maintaining the ability of vertical take-off and landing and perching capabilities that are typical of rotary-wings drones. To navigate tighter spaces, micro aerial vehicles (MAVs) come into play [2,3], an example of which is shown in Fig. 1. Their biggest challenge, apart from to the complex kinematics and unsteady and nonlinear aerodynamics, is devising a light weight power unit that allows for independent, untethered flight.

There is a large pool of technologies available to manufacture miniature devices. The choice depends on requirements such as material properties, feature size, dimensions and shape, as well as the final application of the microfabricated system, e.g. environmental requirements. These miniaturized devices typically require high reproducibility, design flexibility, scalability and multiplexed features. By building parts with additive manufacturing, it is possible to create structures with novel properties that cannot be achieved through more traditional top-down approaches. When manufacturing mesoscale products, where mesoscale represents dimensions in the mm to cm range but features in the μm to mm range in full 3D, neither approach offers a straightforward solution. Top-down micro manufacturing requires very case-specific tools, as well as machines with enough precision and an extensive assembling phase. Additive manufacturing offers a large range of possibilities depending on the specific technology and the materials that can be used. Machines capable of nano-manufacturing often have reduced build volumes that do not allow for mesoscale prints. When the

☆ This article is part of a Special issue entitled: 'NanoSystems 2024' published in Micro and Nano Engineering.
* Corresponding author.

https://doi.org/10.1016/j.mne.2025.100339
Received 11 June 2025; Received in revised form 11 November 2025; Accepted 20 November 2025
Available online 20 November 2025

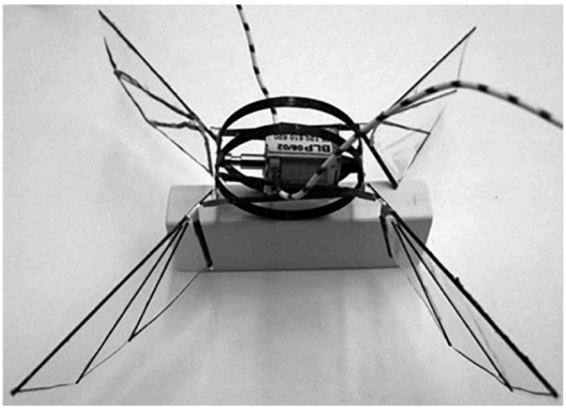

Fig. 1. Prototype of a flapping wing micro-aerial vehicle (FWMAV) [11]. (Used with permission).

build volume falls in the range of mm or cm, the precision is namely in the μm range. Furthermore, the theoretical precision achievable by the printers varies on the basis of the geometry of the print. Features such as thin walls, hollow geometries, the need for supports are all factors that contribute in complicating the manufacturing process and increase the chances of failure. This illustrates a gap in the feasibility of mesoscale products.

The expansion chamber

The challenge of miniaturizing the power unit of MAVs has been explored from various angles in the past decade. Researchers have studied the usage of piezoelectric elements to power flapping wings MAVs (FWMAVs) [4,5], as well as dielectric elastomers (DEAs) [6–8]. Others have investigated the usage of shape memory alloys (SMA) [9]. However, energy and power density are crucial parameters in the design process of an untethered actuator and chemical energy sources show a great potential in that regard. In traditional chemical based engines, mixing procedures and spark-based ignition are widely used. However, there are challenges in resizing these technologies to microscale. The presence of a spark and an ignition phase that, at small scales, is impaired by quenching and heat losses. Catalytic reactions of mono-propellants can be used to solve these issues. In this instance, no mixing is required and the exothermic reaction is triggered by surface contact of the fuel with the catalyst.

An additional obstacle is represented by the layout of a classical fuel-based engine. Its structure typically consists of a cylinder and a piston. The fuel burns in the cylinder and its expansion drives the piston. Leakage between the cylinder and the piston wall is typically dealt with by implementing sealing elements introducing friction. Unfortunately, when reducing the size of a traditional cylinder-piston engine, phenomena like leakage and friction become more dominant, to the point of a theoretical size limit to 0.3 cc [10].

To tackle this limit and use an expansion chamber below the limit size, its concept is changed. The expansion chamber will not be made by separated piston and cylinder, but it will be a monolithic, compliant piece that combines the functions of both parts. This means that leakage is automatically tackled without the need for sealing elements and the accompanying friction. A schematic of the engine is shown in Fig. 2.

Requirements

There is a set of requirements that the compliant expansion chamber must meet to be able to be considered fit for use. First, the expansion chamber needs to be light. For a FWMAV such as the one depicted in Fig. 1, the weight available for the engine unit is, including fuel, limited to 2 g [11]. This is an ambitious goal, but the weight of the actuator is a crucial parameter for success. Second, with a maximum room of 3 cm to host the actuation unit, the need for simplicity plays in favour of maintenance and parts replacement. This is also why integration of functionalities is key to ensure both lightness and compactness. Moreover, due to the wings being driven indirectly through the “thorax” of the FWMAV, the actuator needs to perform a linear motion to deliver the driving force to the mechanism. This implies that implementing rotatory elements, e.g. a miniaturized gear box, would lead to the need of a transmission system between the rotatory and the reciprocating wing motion. Such a solution would greatly increase the number of elements in the actuation and drive down the overall efficiency of the system. In addition, the compliant expansion chamber needs to be compatible with temperatures up to 100 °C, as well as with a humid environment while keeping its flexibility, crucial to the functioning of the actuator.

The compliant expansion chamber design is shown by the model in Fig. 3, with a size of 9.8 mm diameter and 7.5 mm height, and thickness of the lateral wall ranging between 100 μm and 160 μm. The wall is shaped in a zig-zag pattern, resembling an accordion. This feature allows the prototype to compress and expand, as shown in Fig. 4.

Manufacturing technologies and their limitations

Considering these requirements, the manufacturing of the device has been tackled by initially selecting applicable techniques and machines at our disposal. Among these are photopolymerization, injection moulding and multijet printing. For photopolymerization in particular, both stereolithography (SLA) and two-photon lithography (2PP) (see Fig. 5) have been considered. The latter (see Fig. 5d) achieves relevant results in the range of arbitrary 3D nano-structures [12] and it is typically used for design and pattern generation, microneedles [13], nanopillars [14], microfluidic devices [15], MEMS [16] and micro-optics [17]. While providing excellent resolution to achieve features down to 50 nm [18], it

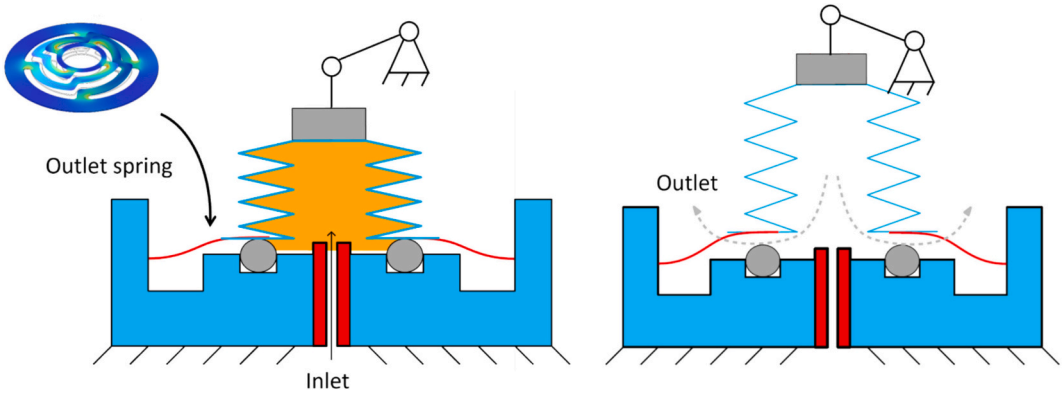

Fig. 2. Functioning scheme of the expansion chamber. On the left, expansion phase. The outlet spring, preloaded, holds the chamber closed until it reaches a predetermined expansion. When the expansion reaches its peak, on the right, the spring opens automatically, releasing the byproducts of the reaction.

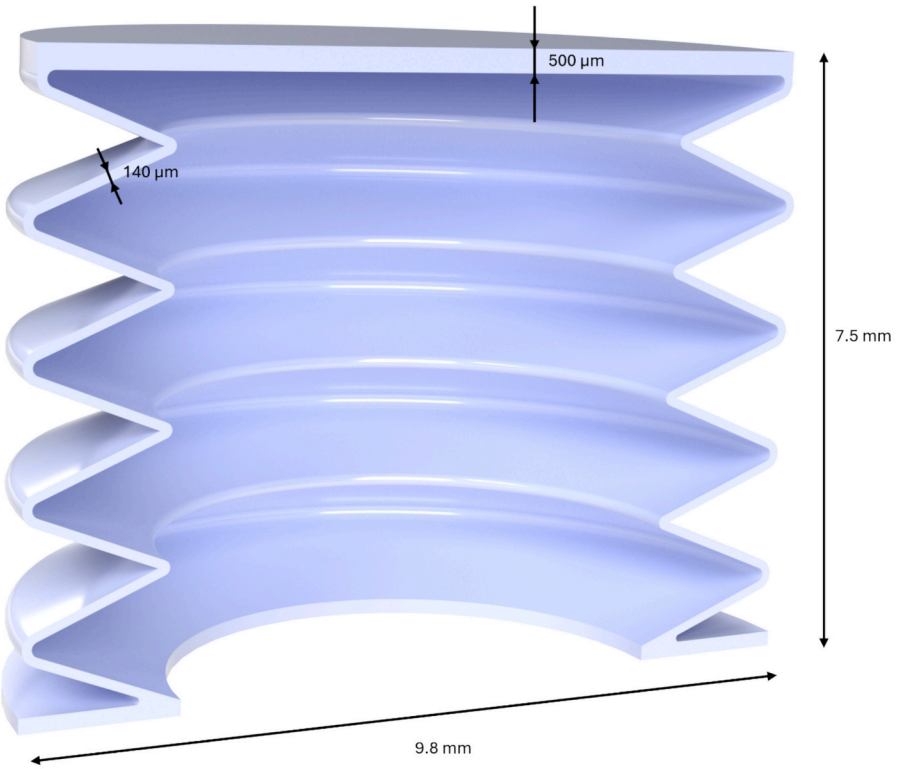

Fig. 3. Rendering of a cross section of the compliant expansion chamber along the vertical plane.

proves not suited to manufacture the overall scale of the object. 2PP offers a variety of lenses with diverse magnification factors that increase printing flexibility, however, using the lowest magnification lens available, the printing area of 1000 µm is still not sufficient for the fabrication of the compliant expansion chamber. A workaround consists in threading the different parts together. However, this method would lead to higher chances of inaccuracies in the threaded areas [19], as well as increasing the printing time to the span of a few days.

Fortunately, this challenge is absent when employing SLA, as the printing area varies greatly between machines and can comfortably host the product. On the other hand, while namely SLA can achieve resolutions down to 8 µm [20], depending on the instrumentation employed, the minimum feature size does not correspond to the theoretical one and is, in fact, significantly larger.

Feature size and dimensional accuracy are affected by multiple aspects of the system, optics, materials and printing process. In a laser-powered SLA machine (Fig. 5a), the spot size sets a lower limit for the smallest feature achievable on the horizontal plane, as well as for dimensional accuracy. Similarly, for a digital light projector (DLP) printer (Fig. 5b), resolution is limited by pixel size. In masked-SLA (MSLA) (Fig. 5c), LCD screens mask the light and the actual image projected onto the resin is typically larger and therefore more blurred than the original pixel. This effect is known as "point spread function" (PSF). Consequently, the power distribution and shape of the light as it hits the resin in these printers has more influence on the smaller feature shape and dimension than the size of the pixels themselves. However, the aspect of this feature will change based on whether it is engraved, embossed, a hole or a channel.

In addition to such parameters, for SLA printed parts there is more to determine effective resolution. The peel forces experienced as each printing layer is pulled from the film during the printing phase, load the part. This can lead to detachments between the last layer and the printed part, or cause deformation of the part.

Depending on the implemented material, overpolymerization also affects print resolution. This is especially problematic when the feature size approaches the printing resolution. Especially, when uv light hits a transparent resin, which is the case for most flexible resins, it scatters, provoking the polymerization of a portion of material outside the material corresponding to the lit pixels. It is however possible to implement a photoabsorber to the resin. It absorbs the wavelength of the uv light and it allows for the confinement of stray and scattered light, helping to minimise the excessive cured material and to comply better with the design dimensions.

Similar to SLA, material jetting technology [21,22] makes use of photopolymers and UV light, but substantially different is the presence of inkjet heads. The minimum feature size for polyjet printers differs greatly between machines and depends mainly on the jet head, but for some of those, it competes with the parameters from SLA. An advantage of this technology is the possibility of embedding multiple materials into one print, therefore increasing design flexibility. However, the printing parameters are mostly fixed, unlike with most SLA printers.

Both material jetting and SLA are among the most accurate and precise 3D printing processes and both of these technologies have been investigated for the manufacture of a mesoscale compliant expansion chamber. An overview of the SLA printers used in the present study is available in Table 1.

Results and discussion

As a consequence of the printing process itself, the thickness of the walls represents a critical point for SLA. The geometry of the expansion chamber is axial-symmetric, with a circular base. This design choice impacts a-priori the minimum thickness achievable. To illustrate this concept, Fig. 6 shows two examples. The first case depicts straight lines in x, y direction, representing a wall with minimal theoretical thickness achievable, that is the pixel size. The second case displays a circular line. In both cases, the two models share the same wall size on the xy plane. It is immediately visible that the first case displays a continuous line in both directions, where every lit pixel has one side completely adjoining the following illuminated pixel. On the other hand, in the second case,

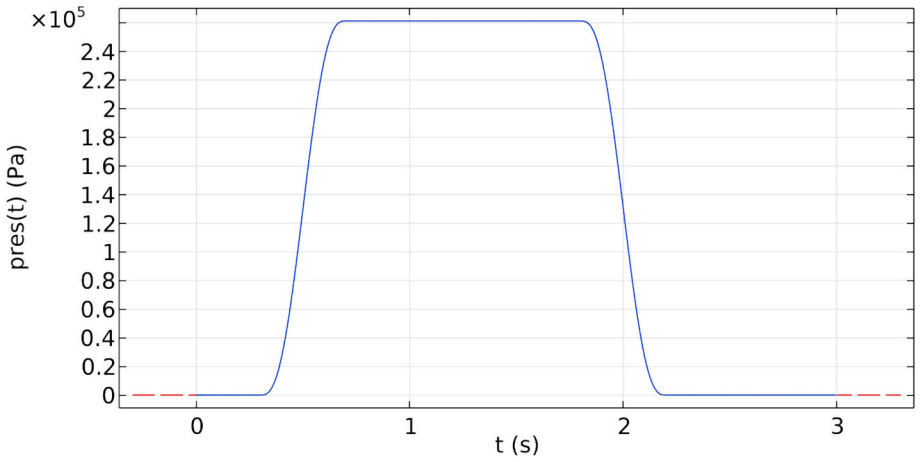

(a)

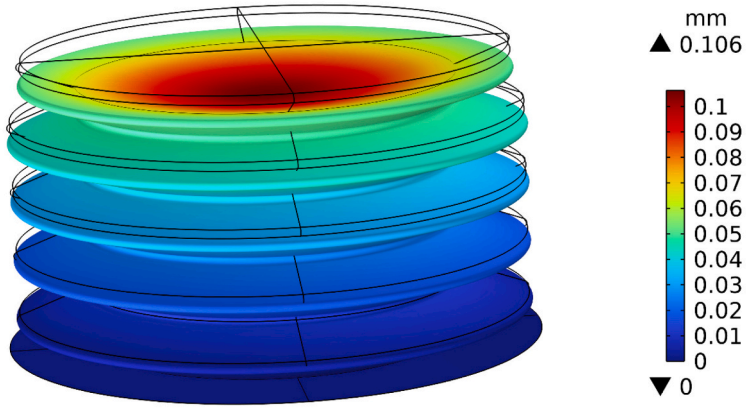

(b)

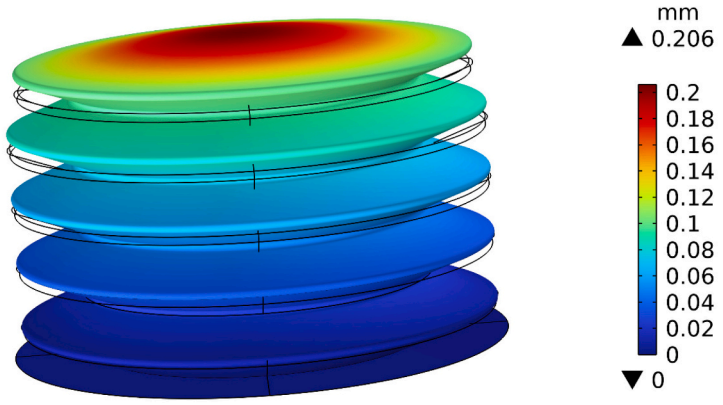

(c)

Fig. 4. FEM simulations (b), (c) of the expansion chamber subjected to a pressure impulse (a), comparable to the rise in pressure that occurs after catalytic decomposition of 4 droplets of H_2O_2.

adjacent pixels share only one corner. Despite keeping the thickness to the theoretical minimum not being recommended, the first scenario might produce a very thin wall. It is likely that the print, if successful, would be difficult to remove intact from the buildplate. However, in the second scenario the model is either not printed, or it presents several hollow sites, due to the lack of physical continuity in the material. Additionally, the anti-aliasing option can be activated to blur the contour defined by the pixels. This happens through adjusting the brightness of the otherwise black pixels outside of the defined contour. While this option can mitigate the discontinuity in the material, it also has the side effect of reducing precision and thickening the contour itself. In addition, the result also depends on the type of material used.

SLA fabrication of mesoscale expansion chamber

The fabrication was carried out with different resins, varying in

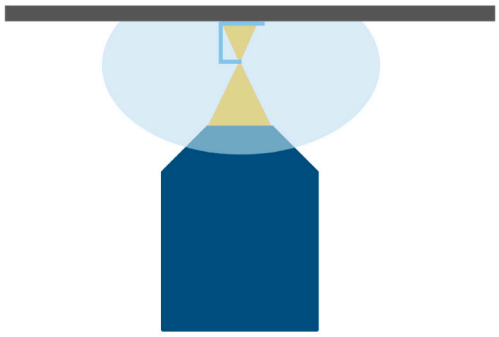

(a) 2PP uses two-photon absorption as a basis principle. Two-photon absorption occurs when an atom or molecule absorbs two photons simultaneously, allowing it to be excited to a higher energy state. The light used in this technology is typically lower-energy, in the near-infrared range. This causes the printing material to solidify only if the resin molecules simultaneously absorb the energy of two photons. This is made possible by focusing the beam in a very small volume inside the photosensitive resin. The laser intensity is maximum at the centre of the focal spot, so that the absorption of the two photons only occurs in this location.

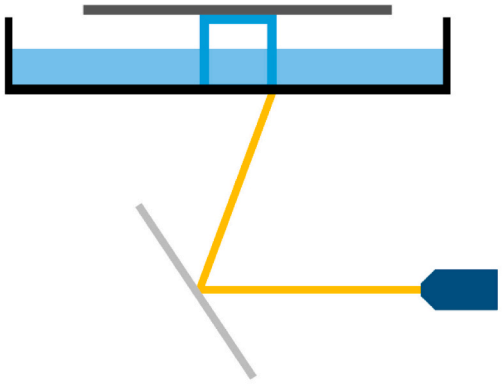

(b) Laser-based SLA, the original SLA, uses a UV laser to draw each layer of the object. Two controllable mirrors aim the laser beam across the print area, polymerizing resin along its path. In order to create a solid object the design is broken down, layer by layer, into a path that makes a set of coordinates for the laser to trace.

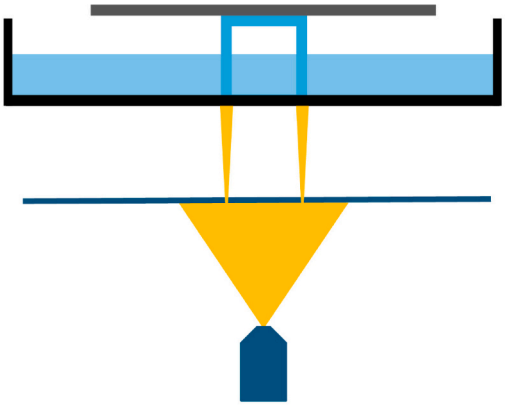

(c) DLP SLA uses a digital projector to shine a pattern of UV light onto the resin. The image of each layer is projected across the entire platform at once. Since the image of each layer is digitally displayed, it is composed of numerous square pixels. After one layer is cured, the platform moves up and the next layer projected. MSLA uses an LED array as its light source. A LCD screen is employed in order to shape the light image from the LED array. Also in this case, the image is made of square pixels.

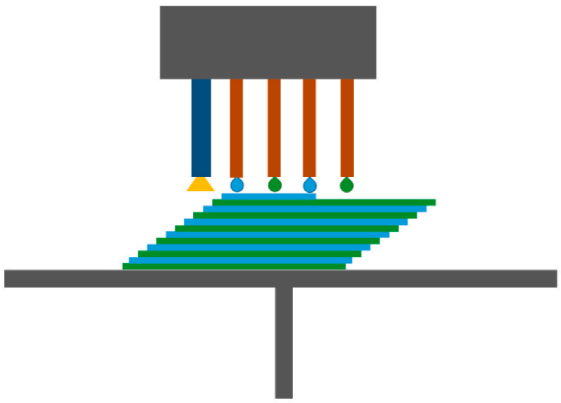

(d) Multimaterial jetting is a type of additive manufacturing technology that prints by jetting microdroplets of photosensitive material on the buildplate. The printing volume is then subjected to uv light exposure that cures the material on the plate. The number of nozzles can vary, but typically multiple nozzles can handle multiple materials, included the support material. In some instances, the buildplate moves along one direction and the header on which the nozzles are mounted moves in two directions, but other machines feature a fixed buildplate and a header that moves in all directions.

Fig. 5. Overview of photopolymerization methods: (a) 2PP, (b) laser-based SLA, (c) DLP and MSLA, (d) Multimaterial jetting.

Table 1
Specifics of different SLA printers used for the present study.

Printer	Technology	Pixel size	xy resolution
Formlabs Form 3+	Laser-powered SLA	85 μm laser spot size	25 μm
Anycubic Photon M3 Premium	DLP	25 μm pixel size	25 μm
Prusa SL1	MSLA	47 μm	47 μm

hardness between 50A , 80A and 70D. The resins of Shore A that were employed were transparent, the resin of Shore D opaque.

At first, the concept was tested with larger scale prototypes, shown in Fig. 7. These prototypes have a height of 2.7 cm, a diameter of 2 cm and a thickness of 5 mm. Specifically, it showed that the geometry was manufacturable with SLA technology and that the prototypes displayed the desired motion when actuated along their axis. After, the prototypes have been miniaturized to the point of reaching the desired specifications and testing with different thicknesses and materials has been carried out.

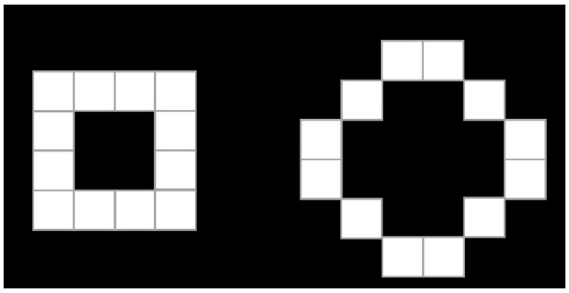

Fig. 6. Descriptive scheme of a square and a circle whose thickness equals pixel size. As it is visible, while the square features a continuous solid line along its contour, the perimeter of the circle displays multiple points with virtually no material, making its contour discontinuous.

The larger scale prototypes display the wanted behaviour. They are capable of compression and extension in a linear motion, their flexibility is preserved over time and outside laboratory conditions. The prototypes keep their mechanical behaviour unaltered for months at room temperature and after exposure to humidity and sunlight. Those prototypes were manufactured with Flexible 80A and Elastic 50A from Formlabs. Given the promising prospect, versions with goal dimensions were manufactured using the same materials. Unfortunately, both materials yielded unflexible prototypes that did not compare in behaviour with their larger scale counterparts. This increased stiffness is largely due to their manufactured thickness turning out a few times larger than the designed thickness, as shown in Fig. 8. The samples made with Flexible 80A from Prusa displayed behaviour comparable to their counterparts made with Formlabs resins and machine. These samples were manufactured both on a Anycubic Photon M3 Premium and a Prusa SL1. No substantial difference was observed in chambers from the two machines with the same material.

Tough 70D from Prusa yielded expansion chambers whose thickness was comparable to the design one. However, the resin proved to be brittle even with curing times reduced to the minimum (2 min UV light at room temperature), leading to the failure of all samples.

To compare the performances of the resins of shore A and D, each with their own drawbacks and advantages, a different geometry, resembling an hourglass, was manufactured as shown in Fig. 9a. This proved that the resins of shore A, like it happened for the larger scaled expansion chambers, are sufficiently compliant to allow the creased areas to flex. This property stays over time. However, shore D materials crack as soon as the prototype is tested for compression or expansion.

The difference in measured dimensions of shore A samples from designed ones can be attributed to the light scattering phenomenon happening in transparent resins. All tested resins from shore A were

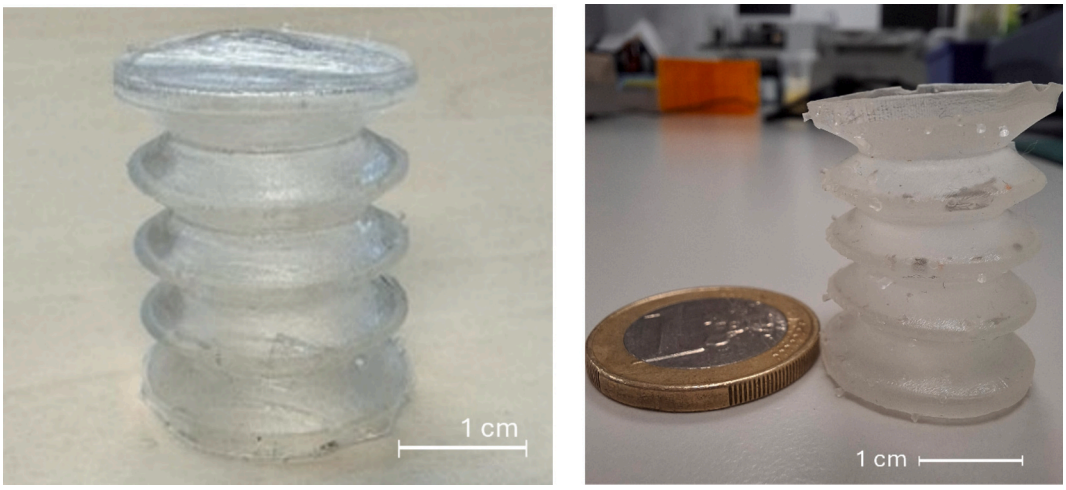

Fig. 7. Larger-scaled compliant expansion chambers. 1 euro coin for scale. The remaining of the support structures are visible in both prints.

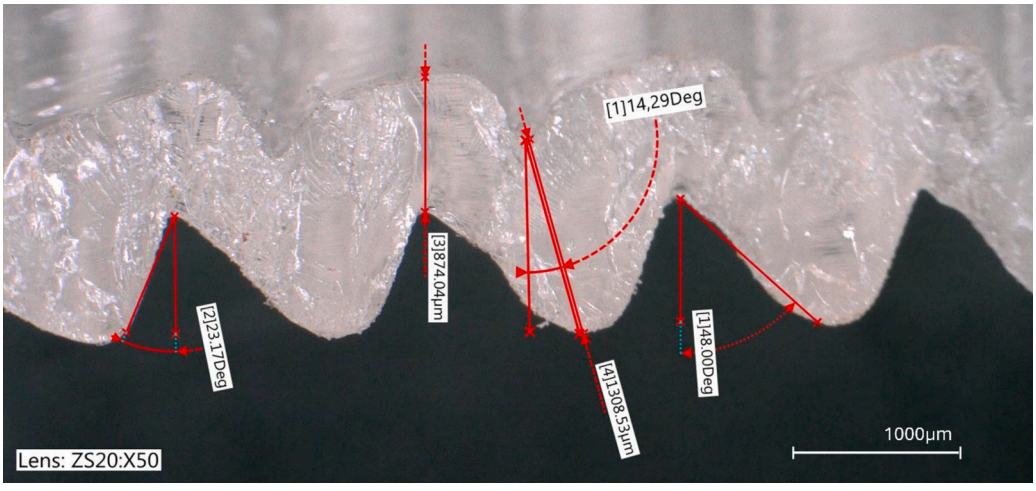

Fig. 8. Microscope image of the cross-section of Flexible 80A expansion chamber. The design thickness was 120 µm and design angles of 22°. It is clear that for this sample, given also the transparent colour, over-polymerization occurred.

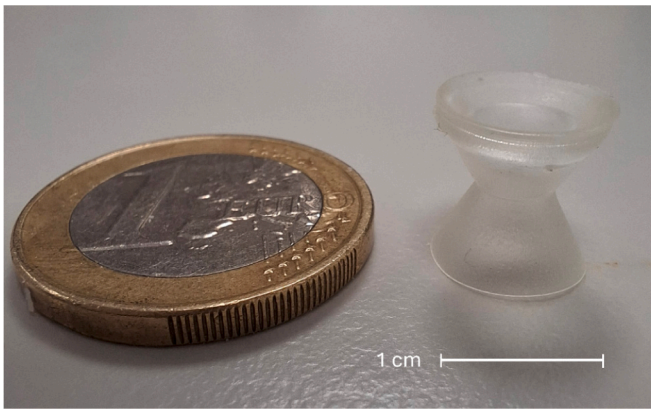

(a)

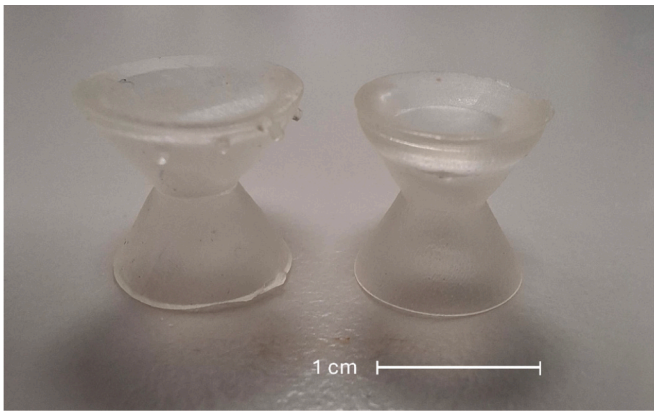

(b)

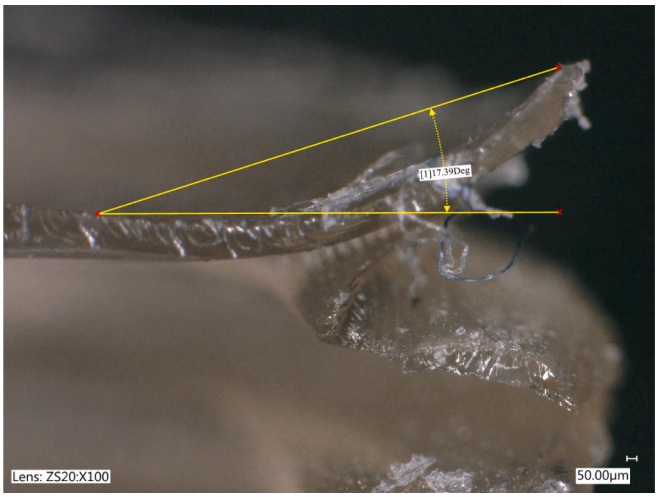

(c)

Fig. 9. Two prototypes of hourglass-shaped compliant expansion chambers. In (a), 1 euro coin for scale. In (b), the difference between a sample printed upright (right side) that displays cup effect. On the left side, a sample printed at an angle to avoid cup effect. The remainders of the supports are visible. In (c), the cup effect is visible at the microscope.

transparent but not the resin from shore D. This consideration led to the implementation of a photo absorber in the Flexible 80A resin, originally transparent. The chosen photo absorber is Sudan Black B (SBB), implemented in a concentration of 0.1 %. The samples produced with such a modified resin present thickness dimensions comparable to designed ones.

As visible from Fig. 9c, even samples produced with SBB corrected resin, display an undesired effect of SLA printing due to the peculiar shape of the object. The expansion chamber is open on one of the flat sides, while the rest, cap and corrugations, are a continuous wall of material. This classifies the geometry as a "cup", making it therefore subject to the so-called "cup effect". This phenomenon is characteristic of SLA printing. When a cup-shaped object is printed, a void portion gets trapped between the already printed base layers on the build plate, the side walls and the bath of resin. Once the z stage moves up after the illumination phase to detach the cured layer from the film, the bubble trapped in between exerts a suction action on the base layers, potentially causing a detachment from the build plate and deformation.

This deformation has been detected almost exclusively on samples made with shore A resins. Samples of shore D material did not display deformation due to the cup effect. A probable reason for this lays in the flexible nature of the shore A resins, which are more prone to deformation in the printing phase and before the post-curing phase. This inconvenience can typically be dealt with in two ways. One method is to introduce holes in the walls to allow the trapped resin or air to escape. The second is to change the orientation of the model on the build plate in order to avoid trapping resin or air to begin with. Clearly, implementing the first solution would hinder the purpose of the expansion chamber. Changing the orientation of the expansion chamber on the build plate meant having to add supports. While supports removal is relatively simple with stiffer resin, the supports can simply be torn off, this step becomes challenging with flexible resins. Considering also the dimension of the thickness of the expansion chambers, the samples are also very delicate to handle before the post-curing phase. While the cup effect was successfully avoided by changing the orientation of the samples, the removal of the supports eventually damages the entirety of the samples or hinders their function. The samples that stayed whole and undeformed after support removal, displayed remnants of the support structure that prevented them from compressing. Reducing the pinhead size of the support structures and head penetration led to failed prints with pinhead size support and head penetration up to 1 mm and 0.4 mm respectively. The minimum values of these parameters that led to successful prints, generated supports whose total removal was not possible without damaging the print.

In view of the diverse combinations of material and machines used, only shore A resins with the addition of SBB had micrometric dimensions comparable to the design. The samples that are taken to the subsequent testing step, suffer from deformation due to the cup effect. It is not expected that this deformation would jeopardize the correct operation of the samples.

Material jetting fabrication

Similarly, material jetting technology was employed for the fabrication of expansion chambers with wall thicknesses varying between 140 µm and 160 µm, with a diameter of 9.8 mm and a height of 7.5 mm.

Two polyjet type printers have been used for this purpose, the J5 MediJet and the Object 350 Connex 3 from Stratasys. These two printers handle different materials and can print samples featuring multiple materials. This attribute proves to be interesting when it allows a customized mixture of materials in the print.

Samples were fabricated with 100 % original materials, with shore hardness ranging from A30, A50 and D80. While the first two have rubber-like properties, the latter displays polypropylene-like material properties. Printing the material Agilus 30 (A30) using the Connex, at the design dimensions was unrealistic, as the material is extremely soft and yielding. Therefore, the samples have been scaled up by a factor of 2. The resulting expansion chambers were exceptionally flexible and retained such property at room condition. However, this feature has some negative implications regarding the incapability of the expansion chambers to deform along their longitudinal axis, as intended. Additionally, the extreme flexibility makes them vulnerable to tearing upon expansion. An interesting property, on the other hand, was displayed by samples printed with Vero (80D). The geometry and dimensions of the

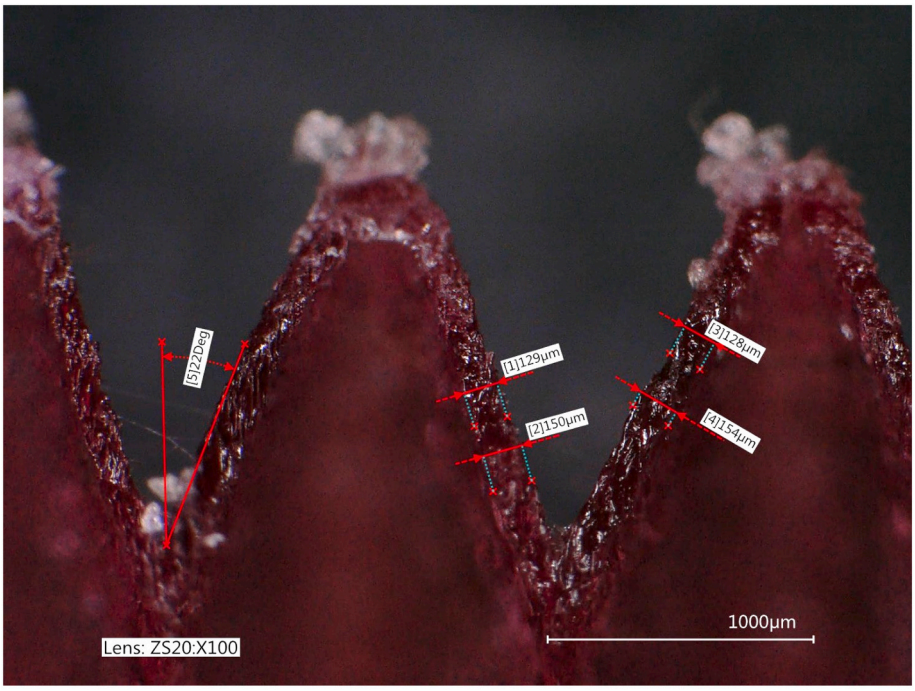

(a)

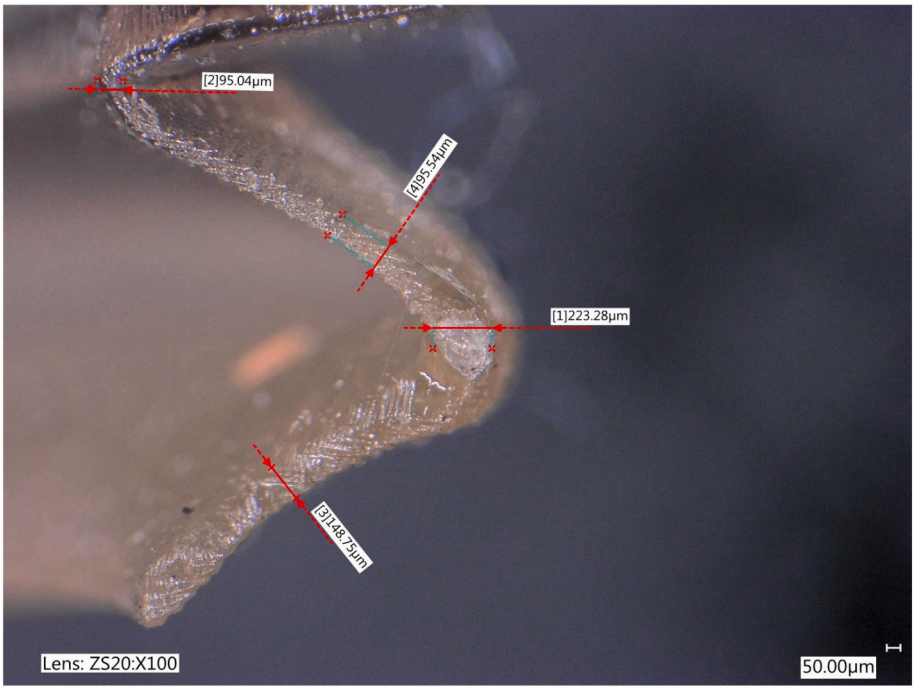

(b)

Fig. 10. (a) Microscope image of the cross-section of Vero 80D expansion chamber. The design thickness was 120 µm and design angles of 22°. (b) Microscope image of the cross section of a sample in SBB-added Flexible 80A, design thickness 140 µm.

samples mirrored the design ones, as it happened in SLA with a comparable material, as shown in Fig. 10a. Upon being kept in a humid environment, these samples are capable of compact compression and extension without breaking. If dried, their behaviour becomes brittle and they break in a similar manner to what was seen with shore D SLA prints. The flexibility property returns when the samples become moist again. UV light exposure does not alter this property.

The two polyjet machines make use of separate support material, unlike the SLA printers. Typically, this material is sacrificial and it is dedicated exclusively to the supporting function. Moreover, the support completely envelops the print. For the Connex the available support material has to be mechanically removed while for the MediJet it is soluble in water. The post-processing methods required to remove such supports is time-consuming in both scenarios and, given the geometry of the devices with enclosed areas, there is the risk of degrading the prints [21]. In the first case, the removal of the support is a long process and, being Agilus30 non-rigid, damaging the device while attempting to remove the supports was a relatively common occurrence. In addition, the complete removal of the support material, given the presence of inner corners, difficult to reach, was not possible and crumbs of support material remained stuck on the inside of the print. On the other hand, the complete removal of the water soluble supports, despite being also lengthy in time, proved to be successful. Depending on the number of samples being simultaneously cleaned of the supports, a number of 5 to 8 cycles in an ultrasound cleaner, of 5 min each, while changing the water at every cycle, is needed for the complete dissolution of the support material. The removal of the external portion of the support is also possible by leaving the samples in water overnight. In that case, a lower number of cycles in the ultrasound cleaner, from 3 to 5, is needed to remove the support on the inside of the prints.

The presence of the water-soluble support, while safe to preserve the devices made with Vero material, hinders a successful final outcome when printing with Elastico (A50) material. As the support material dissolves in water, the creases of the chambers fold on themselves and stick together, yielding a print collapsed on itself as shown in Fig. 11b.

Exploiting the aforementioned capability of the polyjet machines to combine multiple materials in the same print, the expansion chamber was topologically divided in 3 areas, as shown in Fig. 12a. The areas less subject to bending due to extension and compression, were fabricated with the tougher material. The corner areas, more subjected to bending strains, were made with a mixture of Vero and Elastico. These mixtures are a combination of Elastico and Vero at different percentages, creating materials with a range of elastic properties between shore A60, A70 and A80. The final result were samples that dimensionally compare to

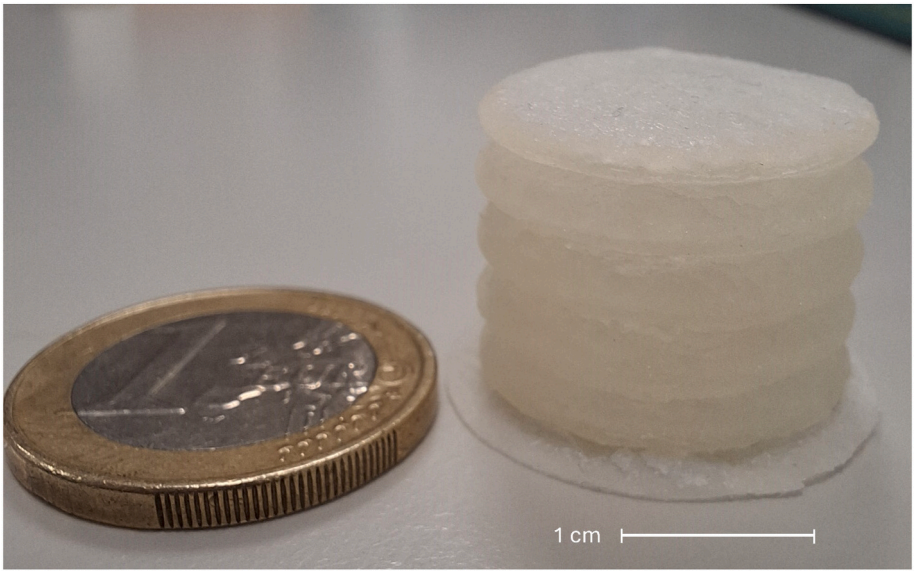

(a)

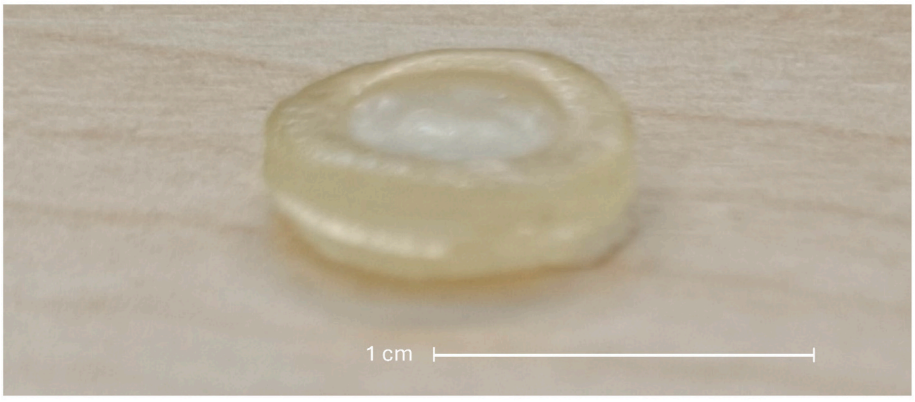

(b)

Fig. 11. Prints made with jetting technology. (a) with Agilus 30A, whose properties allowed for such geometry the minimum scale seen in figure. (b) expansion chamber made wholly of Elastico with material jetting. The supports require dissolving in water and, during the dissolving process, the chamber collapses on itself. This is likely due to the great flexibility of the material that, united with the micrometric thickness, makes the sample unable to hold its own shape during the dissolving process. In addition, water favours the sticking of the folds to one another, leading to such outcome.

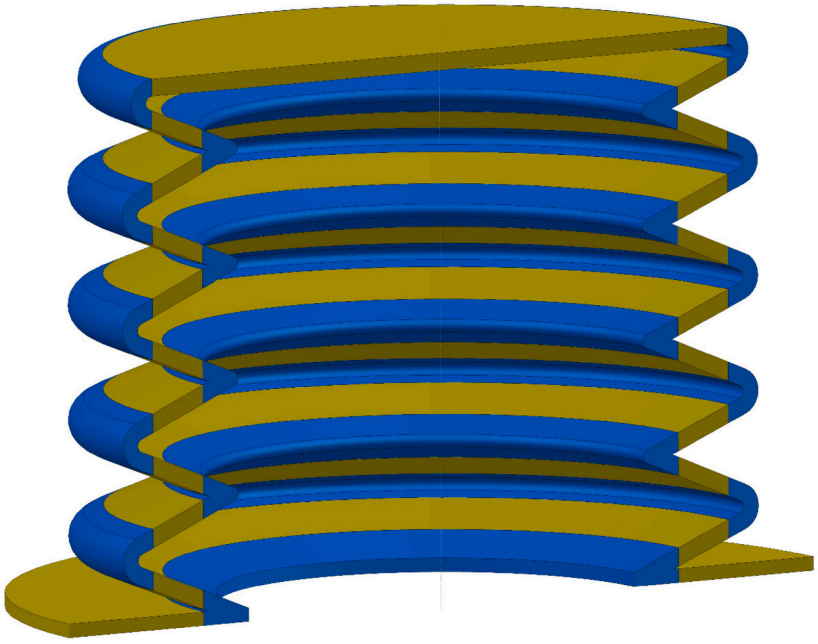

(a)

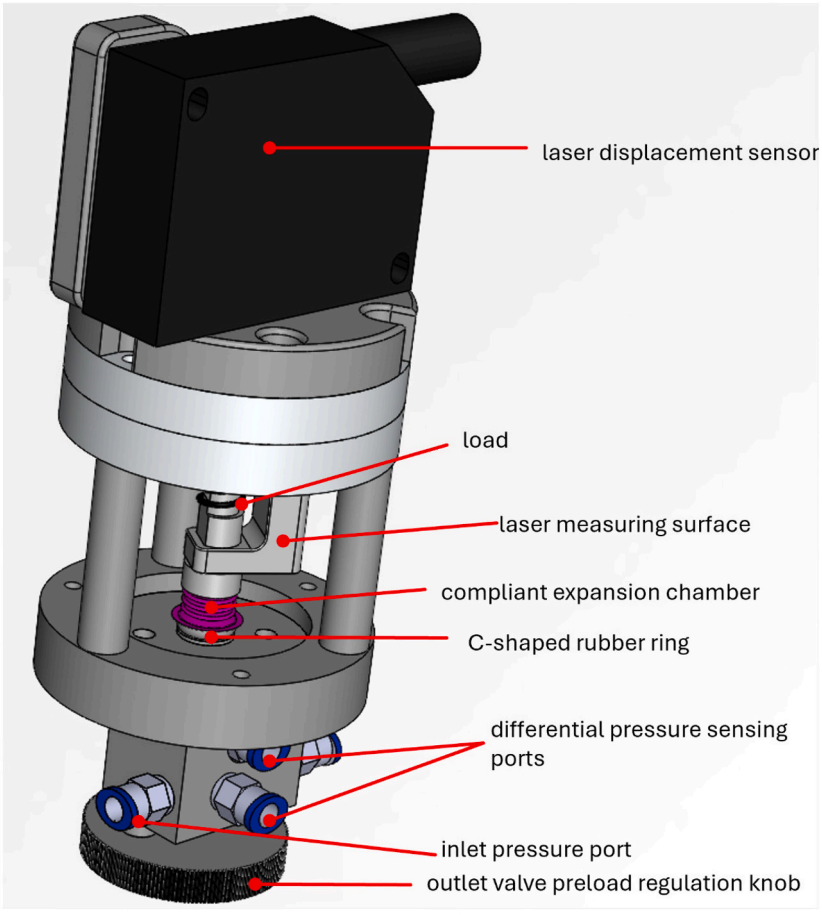

(b)

Fig. 12. (a) Topological division of the expansion chamber in three areas. In yellow, the areas less subjected to bending and therefore fabricated in Vero material (stiffer). In blue, the corner areas more subjected to bending, therefore printed in a more flexible mixture of Vero and Elastico. (b) Scheme of the experimental setup including the expansion chamber, whose dimension are reported in detail in Fig. 3. (c) shows a result of the experiment performed with the setup in (b), where the pressure achieved and the subsequent displacement are shown. (For interpretation of the references to colour in this figure legend, the reader is referred to the web version of this article.)

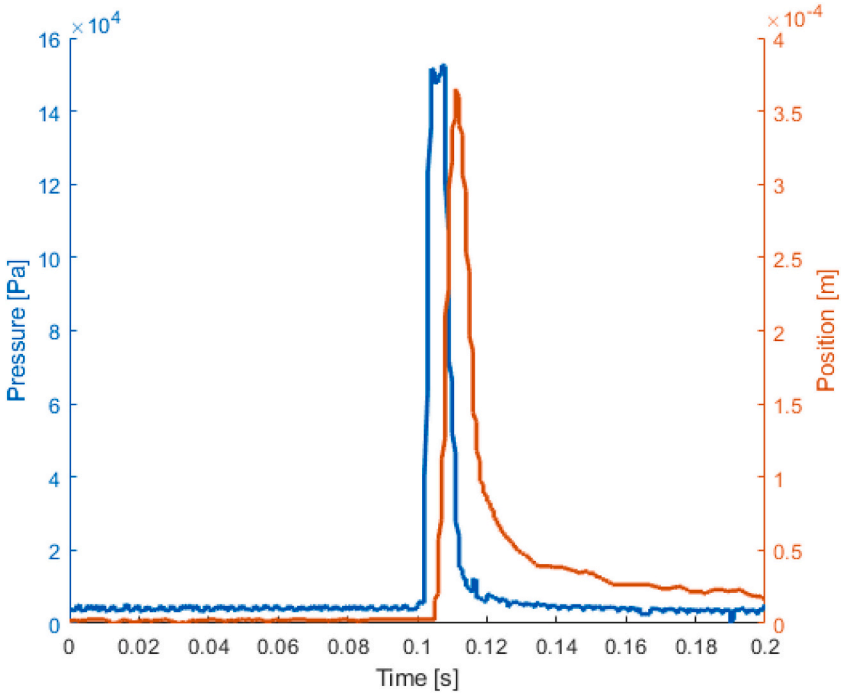

Fig. 12. (*continued*).

design, capable of extension and compression along their longitudinal axis and who keep their flexible property also in a dry environment.

These last samples were tested using pressurization from an external source, with pressure pulses at 1.5 bar. The elongation of the samples was measured through a laser distance sensor. The experimental setup is shown in Fig. 12b and the corresponding measured result in Fig. 12c. No significant difference was observed in the expansion response to single pressure pulse between the multimaterial samples.

Conclusions

Different techniques have been employed for the manufacturing of the mesoscale compliant expansion chamber. The mm-size caused the device to be too large to allow manufacturing with extremely high-precision technologies such as 2PP, necessitating technologies allowing for larger volumes, such as SLA and material jetting. However, the µm feature size proved to be challenging to manufacture accurately with available SLA machines. Similarly, the hollow accordion-like structure was a geometry difficult to fabricate for SLA more than for material jetting. The device is such that it causes a conjunction of typical weaknesses of SLA technology, such as the presence of the cup effect, difficulty in effective supports removal, enhanced danger of print failure due to pull forces and over-polymerization. Devices with up-to-design parameters and desired function were manufactured with material jetting technology. This technology also allows the use of multiple materials in one print, such that it is possible to combine stiffer and more flexible material in different areas of the samples. The obtained devices have been tested for their desired function, measuring the linear displacement of the devices upon internal pressurization. The experiments reported results close to those expected from simulations, of 0.2 mm elongation of the chamber actuated by 1.5 bar of internal pressure pulse. However, SLA technology is experiencing rapid advancements, and among the state-of the art printers that are currently available, the resolution is improved up to the theoretical value of 2 µm. The manufacturing of the compliant expansion chamber prototype could not be tested on such machines. However, problems such as the cup effect and support problems are not solved by improved resolution.

Overall, the manufacture of parts of several millimetres with features of around a 100 µm in arbitrary shapes is not a given for existing manufacturing technologies and requires special attention, both to the manufacturing process and the object design.

Supplementary data to this article can be found online at https://doi.org/10.1016/j.mne.2025.100339.

Declaration of competing interest

The authors declare that they have no known competing financial interests or personal relationships that could have appeared to influence the work reported in this paper.

Acknowledgements

This publication is part of the project “Bio-inspired Micro Aerial Vehicle for sustainable pest control in horticulture - Flappy” with file number RAAK.PRO04.081 of the research program RAAK-PRO that is financed by Regieorgaan SIA, part of the Netherlands Organisation for Scientific Research (NWO).

Data availability

No data was used for the research described in the article.

References

[1] B. Wu, et al., Functional materials for powering and implementing next-generation miniature sensors, Mater. Today 69 (Oct. 2023) 333–354, https://doi.org/10.1016/J.MATTOD.2023.09.001.
[2] R. Wood, et al., An autonomous palm-sized gliding micro air vehicle, IEEE Robot. Autom. Mag. 14 (2) (Jun. 2007) 82–91, https://doi.org/10.1109/MRA.2007.380656.
[3] Y. Yan, F. Song, W. Wang, H. Zhu, J. Sun, Bioinspired tailless FWMAV design for agricultural plant protection in greenhouses, Comput. Electron. Agric. 231 (Apr. 2025) 110021, https://doi.org/10.1016/j.compag.2025.110021.
[4] N.T. Jafferis, K. Jayaram, P.A. York, R.J. Wood, A streamlined fabrication process for high energy density piezoelectric bending actuators, Sens. Actuators A Phys. 332 (Dec. 2021) 113155, https://doi.org/10.1016/j.sna.2021.113155.
[5] N.T. Jafferis, E.F. Helbling, M. Karpelson, R.J. Wood, Untethered flight of an insect-sized flapping-wing microscale aerial vehicle, Nature 570 (7762) (Jun. 2019) 491–495, https://doi.org/10.1038/s41586-019-1322-0.

[6] D. Niteesh, S. Malkurthi, C. Goyal, A.M. Hussain, Fabrication and characterization of a dielectric elastomer actuator based flapping wing, in: FLEPS 2023 - IEEE International Conference on Flexible and Printable Sensors and Systems, Proceedings, Institute of Electrical and Electronics Engineers Inc, 2023, https://doi.org/10.1109/FLEPS57599.2023.10220379.
[7] Y. Chen, et al., Controlled flight of a microrobot powered by soft artificial muscles, Nature 575 (7782) (Nov. 2019) 324–329, https://doi.org/10.1038/s41586-019-1737-7.
[8] R. Pelrine, et al., Dielectric elastomer artificial muscle actuators: toward biomimetic motion, in: *Smart Structures and Materials* 2002*: Electroactive Polymer Actuators and Devices (EAPAD)*, SPIE, Jul. 2002, pp. 126–137, https://doi.org/10.1117/12.475157.
[9] X. Yang, L. Chang, N.O. Pérez-Arancibia, An 88-milligram insect-scale autonomous crawling robot driven by a catalytic artificial muscle, Sci. Robot. 5 (45) (Aug. 2020), https://doi.org/10.1126/scirobotics.aba0015.
[10] E. Sher, I. Sher, Theoretical limits of scaling-down internal combustion engines, Chem. Eng. Sci. 66 (3) (Feb. 2011) 260–267, https://doi.org/10.1016/j.ces.2010.10.005.
[11] J.F. L., H.J. Goosen, Q. Peters, P. Wang, Tiso, F. van Keulen, Resonance based flapping wing Micro air vehicle, in: M. Moschetta, C. Ronfle-Nadaud (Eds.), *International Micro Air Vehicle Conference and Flight Competition (IMAV2013)*, J, ENAC, Toulouse, France, Sep. 2013, pp. 281–288.
[12] A. Sharaf, B. Roos, R. Timmerman, G.-J. Kremers, J.J. Bajramovic, A. Accardo, Two-photon polymerization of 2.5D and 3D microstructures fostering a ramified resting phenotype in primary Microglia, Front. Bioeng. Biotechnol. 10 (Jul. 2022), https://doi.org/10.3389/fbioe.2022.926642.
[13] Z. Faraji Rad, P.D. Prewett, G.J. Davies, High-resolution two-photon polymerization: the most versatile technique for the fabrication of microneedle arrays, Microsyst. Nanoeng. 7 (1) (Sep. 2021) 71, https://doi.org/10.1038/s41378-021-00298-3.
[14] G. Flamourakis, et al., Deciphering the influence of effective shear Modulus on neuronal network directionality and growth cones' morphology via laser-assisted 3D-printed nanostructured arrays, Adv. Funct. Mater. 35 (5) (Jan. 2025), https://doi.org/10.1002/adfm.202409451.
[15] G. van der Velden, D. Fan, U. Staufer, Fabrication of a microfluidic device by using two-photon lithography on a positive photoresist, Micro Nano Eng. 7 (Jun. 2020) 100054, https://doi.org/10.1016/J.MNE.2020.100054.
[16] O. Ulkir, Design and fabrication of an electrothermal MEMS micro-actuator with 3D printing technology, Mater. Res. Express 7 (7) (Jul. 2020) 075015, https://doi.org/10.1088/2053-1591/aba8e3.
[17] S. Steenhusen, F. Burmeister, H.-C. Eckstein, R. Houbertz, in: H. Helvajian, A. Piqué, M. Wegener, B. Gu (Eds.), Two-photon polymerization of hybrid polymers for applications in micro-optics, Mar. 2015, https://doi.org/10.1117/12.2079277, p. 93530K.
[18] M. Emons, K. Obata, T. Binhammer, A. Ovsianikov, B.N. Chichkov, U. Morgner, Two-photon polymerization technique with sub-50 nm resolution by sub-10 fs laser pulses, Opt. Mater. Express 2 (7) (Jul. 2012) 942, https://doi.org/10.1364/OME.2.000942.
[19] A. Ghaznavi, J. Xu, S.A. Hara, micromachines A Non-Sacrificial 3D Printing Process for Fabricating Integrated Micro/Mesoscale Molds 14, 2023, p. 1363, https://doi.org/10.3390/mi14071363.
[20] A.A. Bhanvadia, R.T. Farley, Y. Noh, T. Nishida, High-resolution stereolithography using a static liquid constrained interface, Commun. Mater. 2 (1) (Apr. 2021) 41, https://doi.org/10.1038/s43246-021-00145-y.
[21] E.H. Childs, A.V. Latchman, A.C. Lamont, J.D. Hubbard, R.D. Sochol, Additive assembly for PolyJet-based multi-material 3D printed microfluidics, J. Microelectromech. Syst. 29 (5) (Oct. 2020) 1094–1096, https://doi.org/10.1109/JMEMS.2020.3003858.
[22] V. Gupta, B. Paull, PolyJet printed high aspect ratio three-dimensional bifurcating microfluidic flow distributor and its application in solid-phase extraction, Anal. Chim. Acta 1168 (Jul. 2021) 338624, https://doi.org/10.1016/j.aca.2021.338624.